# Pathologically Reduced Subbasal Nerve Density in Epithelial Basement Membrane Dystrophy Is Unaltered by Phototherapeutic Keratectomy Treatment

Johan Germundsson and Neil Lagali

Department of Clinical and Experimental Medicine–Ophthalmology, Faculty of Health Sciences, Linköping University, Linköping, Sweden

Correspondence: Neil Lagali, Department of Clinical and Experimental Medicine–Ophthalmology, Faculty of Health Sciences, Linköping University, 581 83 Linköping, Sweden;
neil.lagali@liu.se.

Submitted: June 4, 2013
Accepted: February 16, 2014

Citation: Germundsson J, Lagali N. Pathologically reduced subbasal nerve density in epithelial basement membrane dystrophy is unaltered by phototherapeutic keratectomy treatment. *Invest Ophthalmol Vis Sci*. 2014;55:1835–1841. DOI:10.1167/iovs.13-12533

**Purpose.** To investigate the effect of phototherapeutic keratectomy (PTK) treatment on corneal epithelial wing cell and corneal subbasal nerve density in epithelial basement membrane dystrophy (EBMD).

**Methods.** A total of 39 patients with EBMD who underwent PTK treatment, 40 healthy volunteers, and 24 untreated eyes with EBMD were examined with laser-scanning in vivo confocal microscopy (IVCM). Corneal subbasal nerves and epithelial wing cells were manually quantified from IVCM images by two observers, while epithelial wing cells were additionally quantified by a fully automated method.

**Results.** Subbasal nerve density was significantly reduced in untreated (10,164 ± 4139 μm/mm$^2$; $n = 24$) and PTK-treated (10,624 ± 4479 μm/mm$^2$; $n = 39$) EBMD eyes, relative to healthy controls (18,241 ± 4479 μm/mm$^2$; $n = 40$) ($P < 0.001$). Subbasal nerve density in PTK-treated and untreated eyes did not differ ($P > 0.05$). Epithelial wing cell density did not differ between PTK-treated and untreated EBMD eyes, by either manual or automated analysis; however, epithelial wing cell density in PTK-treated EBMD corneas was significantly reduced ($P = 0.008$) relative to healthy corneas, by automated cell counting.

**Conclusions.** Subbasal nerve density in EBMD is reduced by 45% and recovers only to the reduced level in the long term after PTK treatment, whereas epithelial wing cell density in EBMD is not affected by PTK in the long term. Fully automated cell analysis from IVCM images could provide an objective, standardized means to quantify and compare corneal cell densities in future studies.

Keywords: epithelial basement membrane dystrophy, subbasal nerves, phototherapeutic keratectomy, epithelial wing cell

Epithelial basement membrane dystrophy (EBMD), also known as map-dot-fingerprint, Cogan microcystic epithelial, or anterior basement membrane dystrophy, is a common disorder of the anterior cornea that may affect at least 2% of the general population.[1] It is characterized by any combination of maplike geographic patterns, dot patterns, or fingerprint lines in the corneal epithelium, arising due to defective adhesion between the epithelial basement membrane and the collagen of Bowman's layer.[1] These lesions can change in appearance, numbers, and locations over a period of time and can be difficult to detect on routine examination. EBMD has been described as an autosomal dominant trait in several families, but is more commonly found in patients with no known familial inheritance.[2,3] Corneal dystrophies are by definition hereditary; therefore, the term dystrophy is not accurate unless inheritance can be confirmed.

Although most cases of EBMD are asymptomatic, in approximately 10%, symptoms of painful recurrent corneal erosions or degraded vision are present[1] and require clinical attention. Approximately 10% of these patients, however, are unresponsive to conservative treatment measures (such as lubricant ointments and therapeutic contact lenses) and are considered for surgical intervention.[4] In recent years, excimer laser phototherapeutic keratectomy (PTK) has become an increasingly popular surgical option for the treatment of EBMD, due to successful resolution of symptoms documented in a number of studies.[4–8]

In a previous study, we evaluated the outcome of PTK treatment of EBMD and examined clinical and morphological signs of recurrence of the dystrophy after PTK treatment.[8] In that study, it was found that PTK improved vision in patients and reduced the severity of phenotypic changes in the epithelium, likely due to renewed epithelial adhesion complexes after complete surgical removal of the original basement membane.[8] Despite success of the treatment, the pathogenesis of EBMD is largely unknown, and a number of questions concerning the dystrophy and its treatment remain. For example, the corneal subbasal epithelial nerve plexus that gives rise to epithelial innervation[9–11] is located precisely at the interface of the basement membrane and Bowman's layer, an interface that is pathologic in EBMD. How is the epithelial innervation affected by EBMD? We previously reported a partial recovery of subbasal nerves up to 8 months after PTK,[12] but it is unknown if the treatment influences innervation in the long term, and if so, is the influence a positive or negative one? It has also been shown in a previous prospective study that the

density of epithelial cells can be affected by PTK.[12] It is also unknown whether these changes persist in the long term. Furthermore, localized enlargement, deformation, and displacement of epithelial wing cells has been previously observed in corneas affected by EBMD by in vivo confocal microscopy (IVCM).[8] It is unknown whether these perturbations significantly reduce the epithelial wing cell density.

To address these questions, we undertook a detailed analysis of IVCM images of corneal subbasal nerves and epithelial wing cells in the EBMD patient group examined in our previous[8] cross-sectional study. To allow for comparisons, a control group consisting of 40 healthy volunteers was additionally recruited and examined. Finally, we report a new fully automated technique for cell identification and quantitative analysis in IVCM images, which is based on freely available public-domain software. The automated technique is compared with an earlier manual method of analysis.[12]

The specific hypotheses we wished to address in this study were the following:

Hypothesis 1: Epithelial wing cell density and subbasal nerve density in EBMD differ from that of a healthy population.

Hypothesis 2: PTK treatment changes the epithelial wing cell and subbasal nerve density in EBMD eyes in the long term (>1 year postoperative).

Hypothesis 3: A fully automated cell analysis technique can be used to replace manual assessment of epithelial wing cells in IVCM images.

## Materials and Methods

### Patients

Two subject groups were examined for this study. The first group consisted of 39 EBMD patients from a group of consecutive patients treated by PTK in our clinic between 2001 and 2008 inclusive. Follow-up examinations for this group were completed in 2008–2009, and clinical findings were reported in an earlier cross-sectional study.[8] No specific exclusion criteria were applied to the patient group, but systemic diseases and previous ocular pathology were noted at the time of examination. Follow-ups were completed at least 1 year after PTK in all cases except three, where the follow-up was conducted 10 or 11 months postoperatively. Follow-up time did not follow a normal distribution, with a median of 32 months and range of 10 to 100 months. One treated eye from each patient was included in the analysis to investigate the effect of PTK treatment. In 13 cases where patients were operated bilaterally, only data from the right eye were included. To investigate the characteristics of the cornea in virgin (untreated) eyes with EBMD, examination data from 24 nonoperated, asymptomatic fellow eyes (acquired during the same follow-up visit) were also included. IVCM examination was used to confirm the presence of EBMD pathology in these eyes, which, despite being clinically asymptomatic, had varying severity of EBMD morphology as determined by our grading scale.[8] Of the 24 nonoperated fellow eyes, 7, 1, 7, and 9 eyes had grades 0, 1, 2, and 3, respectively (7 of the 39 patients therefore had apparently unilateral EBMD).

The second group was a control group of 40 healthy volunteers, taken from a population of medical students and persons accompanying patients at the Ophthalmology Department, Linköping University Hospital. Volunteers were included based on willingness to provide written consent and were excluded where eye pathology (past or present), corneal haze, or systemic disease known to affect the eye (e.g., diabetes mellitus) was present. Examination included a thorough medical history using a standardized form, best spectacle-corrected visual acuity, and slit lamp examination to rule out ocular pathology. Laser-scanning IVCM was then performed (Heidelberg Retinal Tomograph 3 with Rostock Corneal Module; Heidelberg Engineering, Heidelberg, Germany). Only data from the right eye of healthy volunteers were included.

Recruitment of patient groups commenced after obtaining approvals from the Linköping Regional Human Ethics Committee (applications M151-08 and M172-09). All patients included in the study gave informed consent to participate, and the study adhered to the tenets of the Declaration of Helsinki.

### In Vivo Confocal Microscopy and Image Selection

The central region of the cornea in all subjects was examined by IVCM, by using the procedure described previously.[8] Based on an earlier study,[12] six en face confocal images from each central EBMD cornea were selected for further quantitative analysis. The first three images contained epithelial wing cells approximately 20 to 25 μm posterior to the corneal surface. Clear, representative images of epithelial wing cells were chosen from each cornea in the following manner. The first image had no visible dystrophy in the image frame, whereas the two remaining images had obvious degenerated cells, cystlike features, or map regions typical of EBMD[8,13] visible in the frame. The remaining three images were of subbasal nerve fiber bundles of the subbasal nerve plexus, located immediately posterior to the epithelium. Clear, representative images of subbasal nerves were selected as follows. The first image was chosen from an area with no EBMD morphology visible and where the frame contained the greatest number of visible central subbasal nerves. The remaining two images contained subbasal nerves and EBMD features were present in the image frame. In the healthy volunteer group, six en face confocal images from each central cornea were selected for quantitative analysis. Three images of subbasal nerves and three images of epithelial wing cells were chosen as follows. One subbasal nerve image with the greatest number of visible nerves, and two other representative images from the central cornea with subbasal nerves were selected. Three epithelial wing cell images of good quality from the central cornea were arbitrarily selected.

The selection procedure was chosen to reflect the general epithelial wing cell and nerve density in EBMD, taking into account both obviously affected regions and regions without visible pathology.

### Image Processing and Manual Quantitative Analysis

All images were coded before analysis. ImageJ software (http://imagej.nih.gov/ij/; provided in the public domain by the National Institutes of Health, Bethesda, MD) was used to superimpose a 200 × 100-μm (width × height) rectangle onto each image of epithelial wing cells to highlight a central region where cell borders were most visible. A background subtraction was then applied to the image. Within each selected region (rectangle or square), a band-pass filter was next applied as described previously,[12] resulting in an improved ability to discriminate individual epithelial wing cells (Fig. 1). Images of subbasal nerves were not processed before analysis. Epithelial wing cells and subbasal nerves in all processed images were manually quantified by two independent, masked observers. Epithelial wing cells were quantified using a point-and-click cell-marking and -counting plug-in, whereas subbasal nerves were semiautomatically traced by using a nerve-tracing plug-in to ImageJ, as described previously.[12] Only clear, distinct cells with visible borders were counted. Cells touching the top and right edges of the rectangular region of interest were

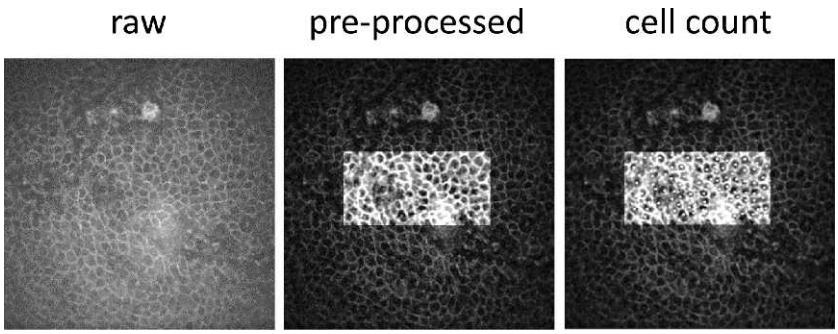


FIGURE 1. Image processing and manual cell-counting method in ImageJ. Raw in vivo confocal microscope images were pre-processed by first band-pass filtering in a central region of interest. Epithelial wing cells were then marked during the counting procedure (a *dot* is used to mark each cell). Image size is 400 × 400 μm, and the region of interest was 200 × 100 μm.

counted, whereas those touching bottom and left edges were excluded (Fig. 1). Epithelial wing cell density (cells/mm$^2$) and subbasal nerve density (total nerve length per image in μm/mm$^2$) were calculated for each image, and images were unmasked. An average of the three density values for each eye and parameter was calculated for each observer. Interobserver repeatability was assessed by the Bland-Altman 95% limits of agreement (LOA).[14] For further statistical analyses, average values for epithelial wing cell and nerve density across both observers were used.

## Procedure for Automated Cell Counting

To investigate a more rapid and objective method for cell analysis, a fully automated cell-counting procedure was developed in the ImageJ platform as follows. A rectangular region of interest was first placed on each image of epithelial wing cells, and the image was background-subtracted and band-pass filtered in a manner identical to the manual procedure (Fig. 2). The image was then cropped to the region of interest, and thresholding was applied using the auto-default setting. The image was then converted to binary ("Make Binary" function), and the "Watershed" function was used to automatically add boundaries, where needed, to separate epithelial wing cells appearing to be adjoined.

Epithelial wing cells in pre-processed images were automatically counted using the "Analyze Particles" function in ImageJ. For epithelial wing cell images, all dark regions (cells) larger than 15 square pixels were counted as cells. Next, automatic image counting was performed twice per image: once with cells touching edges of the image included in the count, and once with cells touching edges excluded (this option is set within the Analyze Particles menu). The final automatic cell count was then taken as the mean of the two counts, to approximate the value that would have been obtained if epithelial wing cells touching only two edges of the image were counted (as in the manual procedure). Finally, the epithelial wing cell density for a given eye was taken as the mean value from automated analysis of the three individual image frames from that eye.

## Statistical Analysis

To test for differences in epithelial wing cell and nerve density across subject groups, one-way ANOVA was applied. Where a significant relationship existed, multiple pairwise comparisons were performed by using the Holm-Sidak method, to isolate significant differences. To test for differences in epithelial wing cell density between analysis methods (manual versus automated), the paired *t*-test was used. Correlation of subbasal nerve density with time was tested with the Spearman rank-order correlation test. Normality of data was determined using the Kolmogorov-Smirnov test. For all tests, a two-tailed level of $\alpha = 0.05$ was considered significant. All statistics were performed with the commercial software SigmaStat 3.5 (Systat Software, Inc., Chicago, IL).

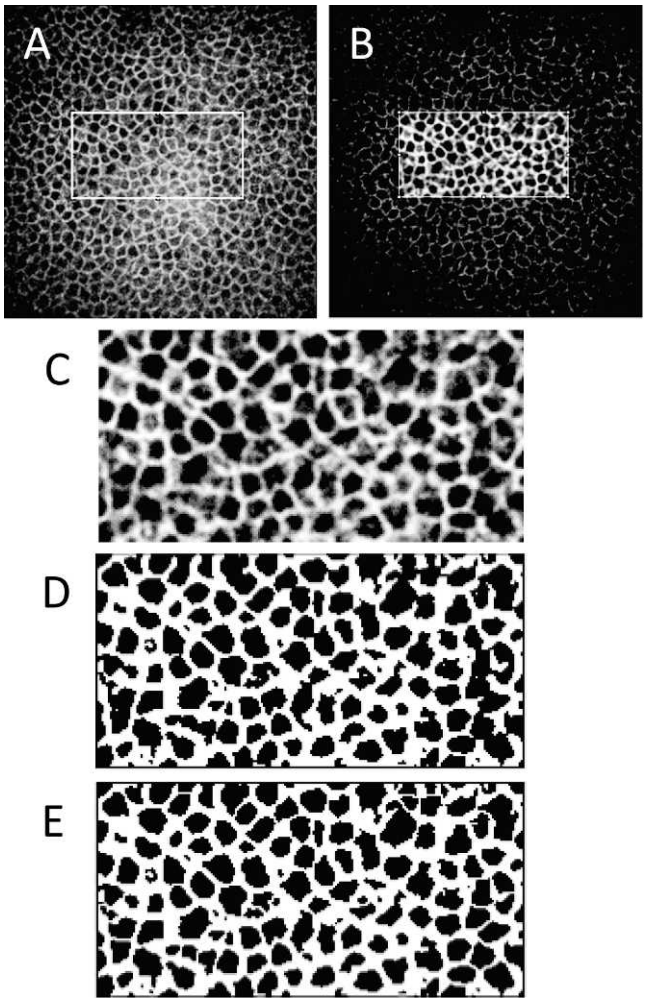


FIGURE 2. Image processing for the fully automated epithelial wing cell analysis procedure. (**A**) A region of interest (*rectangle*) is overlaid on a raw in vivo confocal microscope image of epithelial wing cells. (**B**) Image after background subtraction and band-pass filtering. (**C**) The region of interest is cropped. (**D**) Automatic thresholding is applied. (**E**) The image is binarized and the watershed function is applied to separate adjoined regions into individual epithelial wing cells. *Image size* (**A**, **B**): 400 × 400 μm, (**C**–**E**): 200 × 100 μm.

Investigative Ophthalmology & Visual Science

TABLE. Epithelial Wing Cell and Nerve Density Comparison Between Healthy and EBMD Corneas

| Method | Layer | Healthy, $n = 40$ | EBMD | | Intergroup ANOVA, $P$ |
|---|---|---|---|---|---|
| | | | Fellow, $n = 24$ | PTK-treated, $n = 39$ | |
| Semiautomated | Nerve | 18,241 ± 4479 | 10,164 ± 4139 | 10,624 ± 4479 | **<0.001*** |
| Manual | Wing cell | 5749 ± 388 | 5900 ± 735 | 5990 ± 779 | 0.392 |
| Automated | Wing cell | 6184 ± 387 | 5949 ± 922 | 5833 ± 653 | **0.008†** |
| Intermethod $t$-test, $P$ | | **<0.001** | 0.184 | 0.077 | |

"Wing cell" refers to corneal epithelial wing cells, and "nerve" refers to corneal subbasal nerves. Intermethod $t$-test refers to a paired $t$-test between manual and automated methods of epithelial wing cell density quantification. Data are the mean ± SD. Epithelial wing cell density is expressed as cells/mm$^2$ and subbasal nerve density is expressed as μm/mm$^2$. EBMD corneas are separated into those operated by phototherapeutic keratectomy between 2001 and 2008 and asymptomatic, nonoperated fellow eyes. Bold values indicate results that were statistically significant.

* Subbasal nerve density in healthy corneas was significantly greater than in PTK-treated and fellow corneas in the EBMD group ($P < 0.001$ for both). No difference was detected between PTK-treated and fellow corneas ($P > 0.05$).

† Epithelial wing cell density was significantly reduced in PTK-treated EBMD corneas compared with healthy corneas.

## RESULTS

### Patient Characteristics

Fifty-four percent of EBMD patients were female, and patient age at the time of surgery ranged from 25 to 75 years (mean 54 years). One patient, a 28-year-old male, had type 1 diabetes (without apparent ocular manifestation), and two patients (72- and 75-year-old females) had prior cataract surgery. In the volunteer group of 40 individuals, 53% were female, and the age of the volunteers at examination ranged from 16 to 88 years (mean 59 years).

### Epithelial Wing Cell Density Comparison

Epithelial wing cell and subbasal nerve density in the various subject groups as determined by manual and automated procedures are given in the Table. Epithelial wing cell density in the various groups was normally distributed except for the epithelial wing cell density post-PTK analyzed by the manual method. By both manual and automated methods, no significant difference could be found in the mean central epithelial wing cell density between PTK-treated eyes and nonoperated fellow eyes with EBMD. Epithelial wing cell density in EBMD corneas, regardless of operative status, did not differ from the density found in normal, healthy corneas by manual analysis (Table). By the automated method, however, epithelial wing cell density in PTK-treated corneas was significantly reduced (by approximately 5%) relative to healthy corneas ($P = 0.008$). This difference between manual and automated results was due to a significantly higher epithelial wing cell density in healthy subjects determined by the automated method ($P < 0.001$).

### Subbasal Nerve Density

Subbasal nerve density was normally distributed, and was significantly reduced in EBMD relative to normal, healthy corneas ($P < 0.001$). Subbasal nerve density in EBMD was reduced by approximately 45% compared with healthy corneas. This result was highly significant regardless of whether an EBMD cornea was asymptomatic ($P < 0.001$) or had received prior PTK treatment ($P < 0.001$). Within the group of eyes with EBMD treated by PTK, mean subbasal nerve density was nearly identical to the untreated fellow eyes (Table). Postoperative time was not normally distributed, and subbasal nerve density did not correlate with postoperative time (Spearman correlation coefficient 0.04, $P = 0.82$), indicating no further gain in subbasal nerve density beyond the preoperative level. The distribution of subbasal nerve density among patients and with postoperative time is shown in Figure 3, and typical morphology of the subbasal nerves in healthy and EBMD corneas is shown in Figure 4.

### Interobserver and Intermethod Comparison

Bland-Altman analysis indicated good interobserver agreement for subbasal nerve density with a 95% LOA of ±1789 μm/mm$^2$ (±13% of the mean value). The results of Bland-Altman analysis of epithelial wing cell density are indicated graphically in Figure 5. For epithelial wing cell density, the 95% LOA between observers was ±1276 cells/mm$^2$ (±21%) and the 95% LOA between manual and automated methods was ±1135 cells/mm$^2$ (±19%). A bias toward over/underestimation between observers was evident in the manual technique (Fig. 5A). Averaged values across both observers, however, had minimal bias relative to the automated technique (Fig. 5B). On comparison of subject groups separately, a paired $t$-test between techniques revealed a significantly greater epithelial wing cell density in healthy subjects as determined by the automated method ($P < 0.001$, Table).

## DISCUSSION

Subbasal nerve density was found in this study to be significantly reduced in EBMD corneas compared with a healthy population. Using IVCM, Rosenberg et al.[15] reported diminished subbasal nerves in several cases of EBMD, basement membrane disorder, and recurrent corneal erosions; however, the subbasal nerve density was not quantified. We can now conclude that a general deficit of subbasal nerves (and by extension, epithelial nerves) exists in EBMD. Mean subbasal nerve density was reduced by 45% in EBMD corneas. Unlike epithelial wing cells, which were previously shown to rapidly regenerate after PTK, subbasal nerves are slower to regenerate and remain reduced relative to preoperative levels up to 8 months postoperatively.[12] We therefore hypothesized that PTK influenced subbasal nerve regeneration in the longer term. In this study, subbasal nerves appeared to eventually regenerate to a density comparable to the fellow eye. That the subbasal nerve density did not correlate with postoperative time indicates that after the first postoperative year, subbasal nerves recovered to their preoperative density and were maintained at this level irrespective of postoperative time. Large, long-term studies, ideally with a prospective design, are required to confirm this finding. Limitations of the cross-sectional design were the inability to assess preoperative subbasal nerve density, and the likely differing rates of progression of EBMD

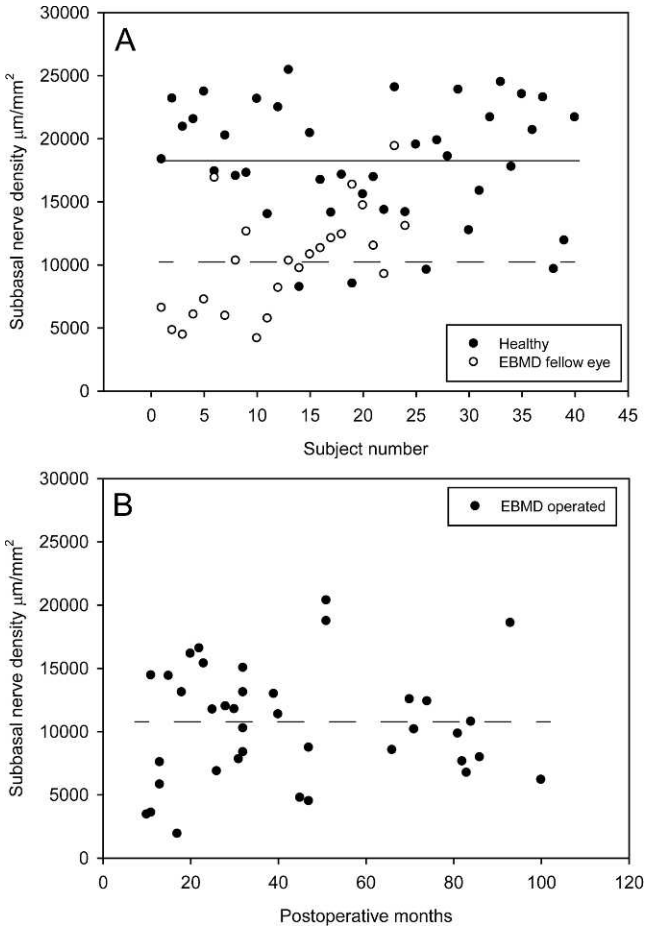


FIGURE 3. Subbasal nerve density in EBMD and healthy corneas. (**A**) Subbasal nerve density in asymptomatic, untreated fellow eyes of EBMD patients (mean value: *dashed line*) was significantly reduced compared with healthy eyes (mean value: *solid line*). (**B**) In EBMD eyes treated by phototherapeutic keratectomy, mean subbasal nerve density (*dashed line*) was nearly identical to untreated eyes. After the first postoperative year, subbasal nerve density did not correlate with postoperative time.

in treated, symptomatic eyes and untreated, asymptomatic eyes.

As the subbasal nerve plexus lies in close proximity to the epithelial basement membrane, it is plausible that the defective adhesion of basement membrane to the underlying collagen and the resulting separation and folding of basement membrane prevents proper innervation, branching, and regeneration. Because subbasal nerves generally regenerate from the periphery after connections to stromal nerves are severed,[16,17] EBMD pathology in the peripheral cornea outside the PTK-treated zone likely limits the degree of central innervation, even in cases in which PTK resolves the pathology centrally. It is important to note, however, that although we did not investigate clinical consequences of the subbasal nerve deficit in EBMD patients, further investigation of ocular surface sensitivity and the tear film is warranted.

A significant but small (5%) decrease in epithelial wing cell density in EBMD relative to healthy corneas was apparent by the automated cell-counting method in this study (but not by manual analysis). The reason for an apparent reduction in density (increase in epithelial wing cell size) after PTK treatment is unclear, and the finding requires further confirmation, ideally in large prospective studies. A reduction of 5%, however, is not expected to be clinically significant. In studies of patients with clinical pathology of the epithelium in conditions such as keratoconus[18,19] and limbal stem cell deficiency,[20] IVCM analysis of epithelial cell density has revealed significant reductions of 23% to 46% relative to healthy subjects. It also should be emphasized that although epithelial wing cell density may change after PTK, grading of epithelial morphology in a previous study[8] showed that PTK improves the overall morphologic appearance in EBMD-affected regions, resolving the characteristic map, dot, and fingerprint features.

We presented here a fully automated technique for epithelial wing cell analysis in IVCM images, which does not require human decision-making. Moreover, the technique is implemented in a popular and freely available image analysis platform, which will hopefully encourage other researchers to adopt the technique. This method could facilitate a more objective approach to quantitative analysis in IVCM and allow comparisons to be made across studies. One potential advantage of the automated technique is in the detection of small but significant relationships that may not be detected by manual analysis (such as epithelial wing cell density reduction after PTK in this study). Further validation of the automated technique in additional patient populations (including healthy subjects) is required to detect possible systematic differences between manual and automated methods, such as the difference in the healthy population found in this study.

The automated algorithm is dependent on several parameters, including the threshold level, exclusion criteria for cell counting, and the treatment of epithelial wing cells touching border regions. Although these parameters could theoretically

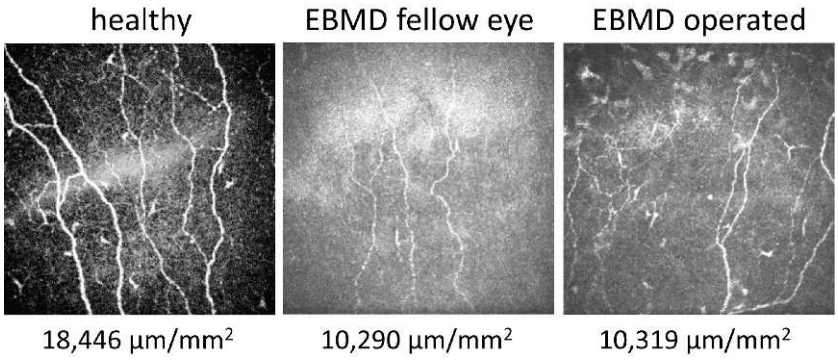


FIGURE 4. Morphologic appearance of subbasal nerves in healthy and EBMD subjects. Compared with healthy corneas (*left*), subbasal nerve density was significantly reduced ($P < 0.001$) in native, asymptomatic EBMD corneas (*center*) and in EBMD corneas operated by phototherapeutic keratectomy (*right*). Subbasal nerve density values by manual tracing (mean of two observers) are given. Images are 400 × 400 µm.

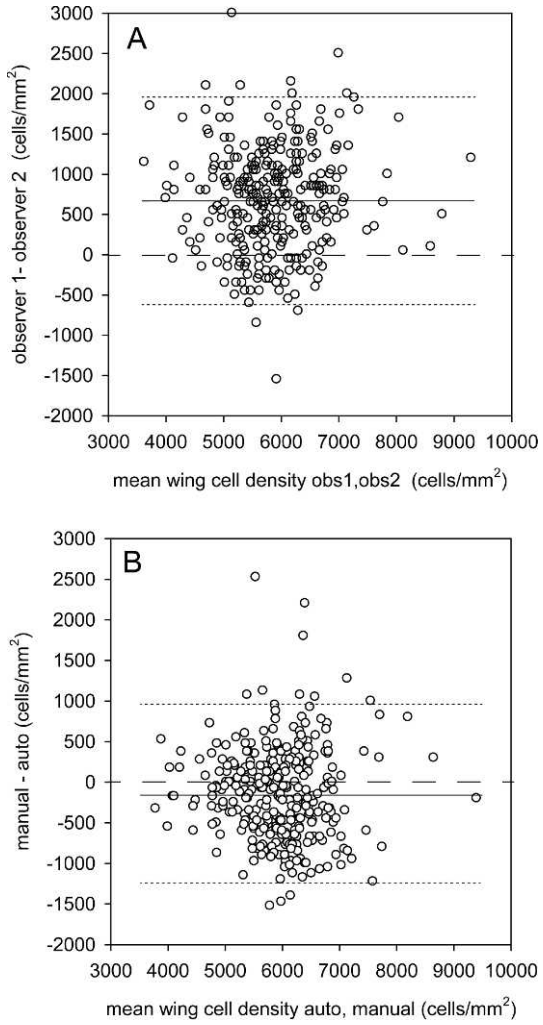


**Figure 5.** Agreement of various methods of epithelial wing cell density determination by the Bland-Altman method. Combined data from all subject groups were used. (**A**) Results from two independent observers indicated a bias toward greater epithelial wing cell density values reported by observer 1. The average level of bias was 673 cells/mm$^2$. (**B**) When results from both observers were averaged, agreement with the automated method was good, with an average bias of 155 cells/mm$^2$ between dual-observer and automated methods. *Dashed lines* indicate perfect agreement, *dotted lines* indicate the 95% limits of agreement, and the average level of bias is indicated by the *solid line*.

be altered to give better agreement with manual counting results for a specific image set of interest, this was not the intent in this study, for two reasons. First, we wanted to provide a fully automated technique for epithelial wing cell analysis that was generally applicable and not tailored to a specific set of images. Second, the manual method was not considered as a "gold standard" to be matched by the automated technique. After performing manual analysis of a large number of images, it became apparent that uncertainties in human image interpretation and human error in cell marking existed, and it was precisely these sources of ambiguity that we wished to avoid by using an automated technique.

It is important to note, however, that the technique we developed was based on the use of images acquired by laser-scanning in vivo confocal microscopy. Cell quantification with images from different nonlaser in vivo confocal microscopes,[21,22] and between nonlaser and laser systems have been compared,[23] with results often differing based on the type of confocal microscope used. A fully automated analysis such as that presented here, however, is readily extendible to nonlaser systems, although some parameters may require adjustment.

Regarding the third hypothesis (can the manual technique be replaced by an automated one), we conclude that it is possible to fully automate the assessment of epithelial wing cells in IVCM images. Bland-Altman analysis of manual counting between observers indicated some level of bias, but when values from both observers were averaged, they more closely matched the automated result. This indicates that the variation between human observers could be overcome by using a fully automated technique.

In summary, although PTK can resolve symptoms and abnormal epithelial morphology in EBMD through renewal of epithelium and its attachment, it does not appear to alter the pathologically reduced epithelial nerve density in EBMD in the long term. Epithelial nerve regeneration is likely guided by peripheral subbasal nerve endings outside the PTK treatment zone.

## *Acknowledgments*

Supported by the Cronqvist Foundation and the County Council of Östergötland (NL). The authors alone are responsible for the content and writing of the paper.

Disclosure: **J. Germundsson**, None; **N. Lagali**, None

## *References*

1. Waring GO III, Rodrigues MM, Laibson PR. Corneal dystrophies. I. Dystrophies of the epithelium, Bowman's layer and stroma. *Surv Ophthalmol*. 1978;23:71–122.
2. Weiss J, Moller H, Lisch W, et al. The IC3D classification of the corneal dystrophies. *Cornea*. 2008;27:1–42.
3. Ehlers N, Moller HU. Dot-map-fingerprint dystrophy—Cogan's microcystic dystrophy—normal reactions of the corneal epithelium? *Acta Ophthalmol*. 1987;182:62–66.
4. Cavanaugh TB, Lind DM, Cutarelli PE, et al. Phototherapeutic keratectomy for recurrent erosion syndrome in anterior basement membrane dystrophy. *Ophthalmology*. 1999;106:971–976.
5. Orndahl MJ, Fagerholm PP. Treatment of corneal dystrophies with phototherapeutic keratectomy. *J Refract Surg*. 1998;14:129–135.
6. Orndahl MJ, Fagerholm PP. Phototherapeutic keratectomy for map-dot-fingerprint corneal dystrophy. *Cornea*. 1998;17:595–599.
7. Sridhar MS, Rapuano CJ, Cosar CB, Cohen EJ, Laibson PR. Phototherapeutic keratectomy versus diamond burr polishing of Bowman's membrane in the treatment of recurrent corneal erosions associated with anterior basement membrane dystrophy. *Ophthalmology*. 2002;109:674–679.
8. Germundsson J, Fagerholm P, Lagali N. Clinical outcome and recurrence of epithelial basement membrane dystrophy after phototherapeutic keratectomy a cross-sectional study. *Ophthalmology*. 2011;118:515–522.
9. Guthoff RF, Wienss H, Hahnel C, Wree A. Epithelial innervation of human cornea: a three-dimensional study using confocal laser scanning fluorescence microscopy. *Cornea*. 2005;24:608–613.
10. Marfurt CF, Cox J, Deek S, Dvorscak L. Anatomy of the human corneal innervation. *Exp Eye Res*. 2010;90:478–492.
11. Al-Aqaba MA, Fares U, Suleman H, Lowe J, Dua HS. Architecture and distribution of human corneal nerves. *Br J Ophthalmol*. 2010;94:784–789.

12. Lagali N, Germundsson J, Fagerholm P. The role of Bowman's layer in anterior corneal regeneration after shallow-depth phototherapeutic keratectomy: a prospective, morphological study using in-vivo confocal microscopy. *Invest Ophthalmol Vis Sci*. 2009;50:4192–4198.
13. Labbé A, Nicola RD, Dupas B, Auclin F, Baudouin C. Epithelial basement membrane dystrophy: evaluation with the HRT II Rostock Cornea Module. *Ophthalmology*. 2006;113:1301–1308.
14. Bland JM, Altman DG. Statistical methods for assessing agreement between two methods of clinical measurement. *Lancet*. 1986;1:307–310.
15. Rosenberg ME, Tervo TMT, Petroll WM, Vesaluoma MH. In vivo confocal microscopy of patients with corneal recurrent erosion syndrome or epithelial basement membrane dystrophy. *Ophthalmology*. 2000;107:565–573.
16. Al-Aqaba MA, Otri AM, Fares U, Miri A, Dua HS. Organization of the regenerated nerves in human corneal grafts. *Am J Ophthalmol*. 2012;153:29–37.
17. Kauffmann T, Bodanowitz S, Hesse L, Kroll P. Corneal reinnervation after photorefractive keratectomy and laser in situ keratomileusis: an in vivo study with a confocal videomicroscope. *Ger J Ophthalmol*. 1996;5:508–512.
18. Mocan MC, Yilmaz PT, Irkec M, Orhan M. In vivo confocal microscopy for the evaluation of corneal microstructure in keratoconus. *Curr Eye Res*. 2008;33:933–939.
19. Yeniad B, Yilmaz S, Bilgin LK. Evaluation of the microstructure of cornea by in vivo confocal microscopy in contact lens wearing and non-contact lens wearing keratoconus patients. *Cont Lens Anterior Eye*. 2010;33:167–170.
20. Deng SX, Sejpal KD, Tang Q, Aldave AJ, Lee OL, Yu F. Characterization of limbal stem cell deficiency by in vivo laser scanning confocal microscopy: a microstructural approach. *Arch Ophthalmol*. 2012;130:440–445.
21. McLaren JW, Nau CB, Kitzmann AS, Bourne WM. Keratocyte density: comparison of two confocal microscopes. *Eye Contact Lens*. 2005;31:28–33.
22. Patel DV, McGhee CN. Contemporary in vivo confocal microscopy of the living human cornea using white light and laser scanning techniques: a major review. *Clin Experiment Ophthalmol*. 2007;35:71–88.
23. Niederer RL, McGhee CN. Clinical in vivo confocal microscopy of the human cornea in health and disease. *Prog Retin Eye Res*. 2010;29:30–58.

Investigative Ophthalmology & Visual Science